

Average structure of an An_{48} plagioclase from the Hogarth Ranges

JOHN D. FITZ GERALD

Department of Earth Sciences, Monash University, Clayton, Victoria, Australia, and
Research School of Earth Sciences, Australian National University, G.P.O. Box 4, Canberra A.C.T. 2601, Australia

JOHN B. PARISE*

Department of Geology, James Cook University, Townsville, Australia, and
Research School of Chemistry, G.P.O. Box 4, Canberra A.C.T. 2601, Australia

IAN D. R. MACKINNON†

Department of Geology, James Cook University, Townsville, Australia, and
Microbeam Inc., Mail Code SN4, NASA Johnson Space Center, Houston, Texas 77058, U.S.A.

ABSTRACT

The average structure ($\bar{\text{C}}$) of a volcanic plagioclase megacryst with composition An_{48} from the Hogarth Ranges, Australia, has been determined using three-dimensional, single-crystal neutron and X-ray diffraction data. Least-squares refinements, incorporating anisotropic thermal motion of all atoms and an extinction correction, resulted in weighted R factors (based on intensities) of 0.076 and 0.056, respectively, for the neutron and X-ray data. Very weak e reflections could be detected in long-exposure X-ray and electron diffraction photographs of this crystal, but the refined average structure is believed to be unaffected by the presence of such a weak superstructure. The ratio of the scattering power of Na to that of Ca is different for X-ray and neutron radiation, and this radiation-dependence of scattering power has been used to determine the distribution of Na and Ca over a split-atom M site (two sites designated M' and M'') in this An_{48} plagioclase. Relative peak-height ratios M'/M'', revealed in difference Fourier sections calculated from neutron and X-ray data, formed the basis for the cation-distribution analysis. As neutron and X-ray data sets were directly compared in this analysis, it was important that systematic bias between refined neutron and X-ray positional parameters could be demonstrated to be absent. In summary, with an M-site model constrained only by the electron-microprobe-determined bulk composition of the crystal, the following values were obtained for the M-site occupancies: $\text{Na}_{\text{M}'} = 0.29(7)$, $\text{Na}_{\text{M}''} = 0.23(7)$, $\text{Ca}_{\text{M}'} = 0.15(4)$, and $\text{Ca}_{\text{M}''} = 0.33(4)$. These results indicate that restrictive assumptions about M sites, on which previous plagioclase refinements have been based, are not applicable to this An_{48} and possibly not to the entire compositional range. T-site ordering determined by $\langle \text{T}-\text{O} \rangle$ bond-length variation— $t_{1\text{o}} = 0.51(1)$, $t_{1\text{m}} \approx t_{2\text{o}} \approx t_{2\text{m}} \approx 0.32(1)$ —is weak, as might be expected from the volcanic origin of this megacryst.

INTRODUCTION

The refinement that is to be reported here on the structure of an An_{48} plagioclase emphasizes details of the Na-Ca cation arrangement. To place the results into context, a brief introduction follows covering some currently accepted aspects of endmember and intermediate plagioclase structures.

Framework configurations of the albite structures ($\text{NaAlSi}_3\text{O}_8$), including details of Al-Si ordering, are well known (Smith, 1974, vol. 1). However, questions have been raised about the modeling of the elongate scattering

distribution associated with the M-cation site, particularly concerning anisotropic thermal motion versus positional disorder (Ribbe et al., 1969). This problem was considered subsequently by Prewitt et al. (1976), Winter et al. (1977), and Winter et al. (1979) through structure determinations at temperatures other than 25°C. Collectively, the refinements demonstrate positional disorder in the M site of high (structural state) albite and thermal motion in the M site of low albite.

Ca-bearing plagioclase is relatively enriched in Al and depleted in Si according to the constraints of charge balance. The increased Al/Si ratio dictates a change in the T-site ordering pattern and hence in the crystal structure. For anorthite ($\text{CaAl}_2\text{Si}_2\text{O}_8$), the c dimension of the $\bar{\text{P}}$ unit cell becomes ~ 14 Å (as opposed to ~ 7 Å in albite) as required by the strict alternation of Al and Si throughout

* Present address: Department of Chemistry, New South Wales Institute of Technology, P.O. Box 123, Broadway, N.S.W. 2007, Australia.

† Present address: Department of Geology, University of New Mexico, Albuquerque, New Mexico 87131, U.S.A.

Table 1. Crystal chemical data for plagioclase sample no. 299B

Chemical composition	Unit-cell parameters
$Na_{0.49}Ca_{0.48}K_{0.03}Al_{1.48}Si_{2.50}O_8$	a 8.179(1) Å
$\Sigma = 1.021$	b 12.880(1) Å
$\Sigma = 3.994$	c 7.112(1) Å
$\rightarrow Ab_{49}An_{48}Or_3$	α 93.44(1)°
	β 116.21(1)°
	γ 90.23(1)°
	V 670.6(1) Å ³

the tetrahedral framework. However, the general framework geometry of anorthite is like that of albite.

Differences that do exist between the albite and anorthite structures result in complexities in plagioclases of intermediate composition. For example, plagioclases with Na content below $\sim An_{60}$ (Smith, 1974, vol. 1, p. 7-8) develop an albite-like C1 structure that gives rise to a reflections (see Smith, 1974, vol. 1, p. 8 for reflection nomenclature). However, plagioclases above $\sim An_{60}$ composition are anorthite-like and produce, in addition to a reflections, b , c , and d reflections that generally sharpen and become more intense with increasing Ca content.

Recently, attention has been focused on the structures of those plagioclases intermediate in composition between albite and anorthite. A superstructure, recognized by the presence of e diffractions, commonly develops in such plagioclases and is often associated with submicroscopic two-phase intergrowths (Grove et al., 1983). Extensive X-ray and transmission-electron-microscope (TEM) observations and consequent superstructure models for plagioclase are reviewed by Smith (1974, vol. 1, p. 150-174), and more recent developments have been summarized by Morimoto (1979). Briefly, these models can be subdivided into two classes: (1) the various shift-density modulation wave models (e.g., Toman and Frueh, 1976a, 1976b; Kitamura and Morimoto, 1977) and (2) the domain models as proposed by, among others, Grove (1977), Horst et al. (1981), and Kumao et al. (1981).

Several refinements of the *substructure* of plagioclase (using only a reflections) have been published for compositions near An_{50} . Klein and Korekawa (1976) refined the structure of a low-structural-state An_{52} plagioclase. Other compositions near An_{50} for which structures have been reported include An_{28} (Phillips et al., 1971) and An_{66} (Wenk et al., 1980). In common with other plagioclases, Al in intermediate plagioclases is concentrated in the T_{10} site relative to the T_{1m} , T_{20} , and T_{2m} sites [nomenclature of Ribbe (1983) is used throughout this paper].

Phillips et al. (1971) showed that the plagioclase M site is elongate and, in subsequent refinements of intermediate plagioclases, split-atom models have been invoked for this site. Various assumptions have been made with respect to the occupancy and chemistry of such split M sites. For example, Klein and Korekawa (1976) chose to divide the M site of an An_{52} plagioclase into two partially occupied atoms, one pure Na, the other pure Ca. In contrast, for An_{66} , Wenk et al. (1980) appear to have nominated two

partially, but unequally, occupied M sites each with a Na/Ca occupation ratio of 34/66. In both of these refinements, the final isotropic thermal parameters for the two M sites have markedly different values, despite the expectation that, for cations with similar ionic radii and with similar coordination, isotropic temperature factors should also be similar.

In this paper, we test the applicability of the above models to the An_{48} structure by deriving, with as few assumptions as possible, the chemistry of a split-atom M site. We report the average structure for An_{48} plagioclase determined from measured intensities of the sublattice (a) reflections. Careful refinements using only sublattice reflections, like those we report, yield structures that must include the averaged effects of positional and/or compositional modulations, if present. Therefore, while definitive solution of superstructures can only be derived using difference and superlattice reflections, general inferences (about the nature of superstructures) can nevertheless be made from refinements using sublattice reflections.

EXPERIMENTAL TECHNIQUE

Sample

The starting material is one of a group of plagioclase megacrysts of intermediate composition weathered from basalt flows in the Hogarth Ranges, northern New South Wales (R. H. Vernon, pers. comm., 1976). The irregularly shaped crystals are pale-yellow, glass-clear, and 1-2 cm³ in volume. The (010) cleavage is moderate while (001) is weak. X-ray fluorescence and electron-microprobe analyses of plagioclase from this source confirm that individual crystals are chemically homogeneous. No fine-scale intergrowth, superlattice, or crystal defects could be identified by TEM or X-ray topography (A. C. McLaren and D. B. Marshall, pers. comm., 1976).

The crystal selected for structure determination (specimen no. 299B) has been examined in detail by the following techniques:

1. The chemical composition given in Table 1 was determined by electron-microprobe (energy-dispersive) analysis.

2. In standard petrographic thin sections, no. 299B appears featureless, except for occasional planar boundaries that mark changes in extinction angle up to 1°, suggestive of growth zoning with compositional variations of ~ 1 mol% An [Deer et al., 1966, Fig. 122, (001) section]. The optic axial angle, measured orthoscopically (Bloss, 1981), is 78.3°, but is not diagnostic of structural state in compositions near An_{50} .

3. The unit-cell parameters (Table 1) have been derived from 57 peak positions ($13^\circ < 2\theta < 84^\circ$) measured on a Philips X-ray powder diffractometer using filtered $CuK\alpha$ radiation and a scan rate of 0.1° 2θ /min. Unit-cell parameters were calculated using the methods of Appleman and Evans (1973). Parameter values indicate an intermediate to high structural state when recast according to the methods of Kroll (1983).

4. $0kl$ precession photographs of no. 299B plagioclase, taken with Zr-filtered $MoK\alpha$ radiation over 10-d exposures, contain very weak and diffuse e reflections. The e reflections in no. 299B appear similar to those presented in a precession photograph of an An_{66} plagioclase by Wenk (1978, Fig. 1a). Faint streaks at half-integral values of l lie parallel to b^* in these $0kl$ precession exposures, whereas reflections on long-exposure $hk0$ Weissenberg photographs are centered on very weak streaks subparallel to the c axis. Diffuse reflections were not included in the structure refinement.

Table 2. Definitions for R factors and goodness-of-fit (GOF) used in the text

Symbol	Formula
R	$\sum(F_o - F_c)/\sum F_o^2$
R_w	$\sum w(F_o - F_c)^2/\sum wF_o^2$
R_2	$[\sum(F_o^2 - F_c^2)^2/\sum F_o^2]^{1/2}$
R_{2w}	$[\sum w(F_o^2 - F_c^2)^2/\sum wF_o^2]^{1/2}$
GOF	$[\sum w(F_o^2 - F_c^2)^2/(m - n)]^{1/2}$

Note: F_o = observed structure factor, F_c = calculated structure factor, w = weight assigned to each observation, m = number of observations, n = number of refined parameters.

5. To determine whether measured reflection intensities might be affected by subsolidus microstructures, thin foils from sample no. 299B were examined by TEM. Weak diffuse e reflections were associated with faint streaks in electron diffraction patterns, and barely perceptible linear contrast was detected on the scale of $\sim 100 \text{ \AA}$ in darkfield images using a reflections. No lamellae (Hashimoto et al., 1976) could be distinguished. Formation of darkfield images from e reflections was precluded by lack of intensity in these superstructure diffractions. Thus, spatial variation of the weak superlattice development could not be investigated directly.

Neutron experiment

The crystal used for data collection, measuring $0.31 \times 0.35 \times 0.37 \text{ cm}$, was cut from the megacryst no. 299B and mounted on the ω -TANA diffractometer at the HIFAR installation of the Australian Atomic Energy Commission. A total of 5177 reflections ($0.0777 < \sin \theta/\lambda < 0.834$) were collected at $\lambda = 0.9891 \text{ \AA}$ using a symmetrical $\omega - 2\theta$ step scan method with background measurements on both sides of each peak. After compensation for the effects of Lorentz factor and absorption ($\mu = 0.28 \text{ cm}^{-1}$) on the 3185 unique reflections of space group $C\bar{1}$, the data set was further reduced, by combination of $hkl-h\bar{k}\bar{l}$ pairs to a total of 2698 reflections.

The function R_{2w} (Table 2) was minimized in program LINUS (Coppens and Hamilton, 1970) using structure-factor weights w set to $1/\sigma^2(F_o^2)$. The various stages of refinement are detailed in later sections. Neutron-scattering lengths from Bacon (1974) were used in the structure refinements. Final atomic parameters with their estimated standard deviations (esd's) are listed in Table 3.

X-ray experiment

A regular-sided fragment measuring $0.019 \times 0.021 \times 0.021 \text{ cm}$ was cleaved from a thin polished slab of megacryst no. 299B, the source of the neutron crystal. A total of 2955 unique reflections ($0.0777 < \sin \theta/\lambda < 0.806$) were collected on a Philips PW1100 diffractometer using monochromated $\text{MoK}\alpha$ radiation and an $\omega - 2\theta$ step scan with background measurements at the upper and lower scan limits for each peak. Reflection intensities were processed using the program of Hornstra and Stubbe (1972), and a total of 2557 reflections satisfying the condition $I > 3\sigma(I)$ were accepted. Corrections for Lorentz, polarization, and absorption ($\mu = 9.33 \text{ cm}^{-1}$) effects were applied.

Program LINUS was used to minimize the function R_{2w} with structure-factor weights set equal to $1/\sigma^2(F_o^2)$. Refinement details follow. X-ray scattering factors for neutral atoms (Cromer and Waber, 1974) were used in the refinement. Final atomic parameters with esd's are listed in Table 3.

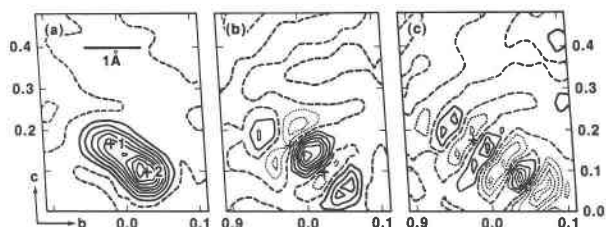


Fig. 1. Difference Fourier sections through the no. 299B plagioclase M site. All plots are b-c sections at $a = 0.26$ for various stages of X refinement. See text for details; section (a) was computed during refinement stage 3, (b) during stage 4, and (c) following stage 5. Contour intervals (in electrons/Å³) for these sections are (a) 2.349, (b) 0.830, and (c) 0.154. Lines representing negative contours are dotted, those for zero contours are dashed, and those for positive contours are solid. Label 1 identifies the final refined position of atom M' , 2 likewise for M'' .

RESULTS AND DISCUSSION

Determination of M-site chemistry

An M-site model involving positional disorder has been used with some success in the high albite structure (Prewitt et al., 1976). Such simple split-atom models can be adapted to suit the mixed-cation chemistry of an An_{48} structure by incorporation of dual Na-Ca occupancy in the M sites. In order to accomplish this, we first assume that the residual on difference Fourier maps can be represented by two partially occupied M sites with equal isotropic temperature factors. This assumption is supported by the observation that the base widths of the peaks representing the M' and M'' sites in the difference Fourier map are approximately equal (Fig. 1a). Determination of Na and Ca occupation of the two M sites follows from the above assumption, because the ratio of the scattering powers of the two partial sites can be taken to equal the ratio of the heights of the two difference Fourier peaks. For the An_{48} of sample no. 299B, the calculated peak-height ratios were found to be (see refinement procedure, stage 3) $M'/M'' = 0.71(4)$ for neutron data and $M'/M'' = 0.65(4)$ for X-ray data, where M' is the label assigned to the peak with the smaller residual. Let the "scattering power" of a Ca atom for either neutron (N) or X-radiation (X) be

$$S_{\text{Ca}}^{\text{N}, \text{X}} = \sum_{i=1}^n f(\text{Ca})_i^{\text{N}, \text{X}} / n, \quad (1)$$

where n = number of reflections in the appropriate data set. $f(\text{Ca})^{\text{N}} = b_{\text{Ca}}$ = neutron-scattering length for Ca (which is independent of $\sin \theta/\lambda$, and therefore of i). $f(\text{Ca})^{\text{X}}$ = atomic scattering factor for Ca calculated for the $\sin \theta/\lambda$ value of the i th observation in the X-ray data set. Similar expressions can be written for the Na atom. It follows that $S_{\text{Ca}}^{\text{N}} = b_{\text{Ca}}$ and $S_{\text{Na}}^{\text{N}} = b_{\text{Na}}$, whereas $S_{\text{Ca}}^{\text{X}} = 8.223e$ and $S_{\text{Na}}^{\text{X}} = 4.029e$; e = the charge on an electron.

If $\Sigma_{M'}$ is the total occupancy of the M' site and $\text{Ca}_{M'}$ denotes the number of Ca atoms in the M' site (with $\Sigma_{M'} = \text{Ca}_{M'} + \text{Na}_{M'}$), then the peak ratio

Table 3. Final refined parameters for An_{48} plagioclase (sample no. 299B) representing structures derived from X-ray and neutron experiments

	X	Y	Z	B_{eq}	β_{11}	β_{22}	β_{33}	β_{12}	β_{13}	β_{23}
X-ray parameters refined with isotropic extinction (program LINUS)										
M'	0.26775(12)	-0.01756(9)	0.16714(15)	2.31	417(12)	628(8)	1081(22)	-175(8)	347(14)	-391(10)
M''	0.271167(7)	0.02751(5)	0.10131(10)	2.09	447(8)	411(4)	1173(15)	130(5)	70(9)	-267(6)
$T_{1,o}$	0.00676(4)	0.16413(2)	0.21481(4)	0.86	396(4)	154(1)	416(6)	-46(2)	166(4)	30(2)
$T_{1,m}$	0.00323(3)	0.81648(2)	0.23087(4)	0.87	407(4)	166(1)	392(6)	77(2)	170(4)	27(2)
$T_{2,o}$	0.68625(3)	0.10900(2)	0.31833(4)	0.84	353(4)	117(1)	546(6)	10(2)	147(4)	15(2)
$T_{2,m}$	0.68191(3)	0.87882(2)	0.35629(4)	0.82	351(4)	118(1)	528(6)	16(2)	156(4)	50(2)
$OA1$	0.00424(10)	0.13009(6)	0.98124(12)	1.76	1112(15)	310(5)	719(17)	74(6)	562(13)	104(7)
$OA2$	0.58250(9)	0.99185(5)	0.27843(11)	1.24	501(11)	159(3)	872(16)	0(5)	207(11)	69(6)
OB_o	0.81416(10)	0.10547(5)	0.19152(13)	1.68	778(13)	221(4)	1357(20)	-45(6)	606(14)	-2(7)
OB_m	0.81622(10)	0.85266(6)	0.24473(14)	2.10	789(13)	298(5)	1803(24)	57(6)	713(15)	-73(9)
OC_O	0.01478(9)	0.29124(6)	0.27976(12)	1.62	696(12)	244(4)	1057(18)	-72(6)	370(13)	36(7)
OC_m	0.01469(10)	0.68743(6)	0.21517(12)	1.67	718(12)	254(4)	847(17)	144(6)	148(12)	-22(7)
OD_o	0.19740(10)	0.10866(5)	0.38381(11)	1.58	689(12)	242(4)	725(16)	29(6)	76(12)	68(7)
OD_m	0.18965(10)	0.86665(6)	0.42927(12)	1.90	681(12)	279(4)	948(18)	31(6)	-37(12)	-61(7)
Neutron parameters refined with type I anisotropic extinction (program RFINE4)										
M'	0.26809(50)	-0.01884(47)	0.16802(64)	2.99	680(50)	790(38)	1366(73)	-217(36)	509(52)	-404(42)
M''	0.27180(32)	0.02701(27)	0.10219(44)	2.59	547(32)	528(19)	1478(55)	176(19)	160(34)	-342(25)
$T_{1,o}$	0.00694(14)	0.16420(9)	0.21481(15)	0.99	462(15)	183(6)	479(16)	-35(7)	210(12)	29(7)
$T_{1,m}$	0.00346(14)	0.81651(9)	0.23115(14)	1.01	474(14)	192(5)	473(16)	94(7)	214(12)	29(7)
$T_{2,o}$	0.68601(13)	0.10893(8)	0.31813(15)	0.98	417(14)	151(5)	607(16)	33(6)	195(12)	25(7)
$T_{2,m}$	0.68193(13)	0.87892(8)	0.35638(14)	0.95	403(14)	156(5)	570(16)	28(6)	199(12)	44(7)
$OA1$	0.00387(13)	0.13025(8)	0.98101(12)	1.89	1141(15)	352(5)	750(14)	86(7)	582(12)	103(7)
$OA2$	0.58279(10)	0.99186(6)	0.27868(12)	1.34	564(11)	183(4)	930(14)	10(5)	270(10)	75(6)
OB_o	0.81405(12)	0.10547(8)	0.19149(14)	1.81	830(14)	268(5)	1365(18)	-45(6)	646(13)	-7(7)
OB_m	0.81627(13)	0.85251(9)	0.24428(17)	2.27	829(14)	361(6)	1864(23)	81(7)	777(15)	-67(9)
OC_O	0.01490(12)	0.29097(8)	0.27964(13)	1.76	764(13)	272(5)	1135(16)	-57(6)	411(12)	40(7)
OC_m	0.01466(12)	0.68761(8)	0.21573(13)	1.80	757(13)	288(5)	920(15)	166(6)	194(11)	-9(6)
OD_o	0.19785(12)	0.10857(7)	0.38416(12)	1.71	762(13)	284(5)	749(14)	36(6)	127(11)	69(6)
OD_m	0.18964(13)	0.86653(8)	0.42901(13)	2.06	770(13)	321(5)	970(16)	36(7)	4(12)	-69(7)

Note: Estimated standard deviations (esd's) of each parameter are given in parentheses. B_{eq} = isotropic equivalent temperature factor (\AA^2). β_i = anisotropic temperature factor ($\times 10^3$).

$$\left| \frac{M'}{M''} \right|^{N,X} = \frac{Ca_{M'} S_{Ca}^{N,X} + Na_{M'} S_{Na}^{N,X}}{Ca_{M''} S_{Ca}^{N,X} + Na_{M''} S_{Na}^{N,X}}. \quad (2)$$

Since the values of $(Ca_{M'} + Ca_{M''})$ and $(Na_{M'} + Na_{M''})^1$ are known from the chemical analysis of this crystal, Equation 2 can be rewritten as

$$\frac{M'^{N,X}}{M''} = \frac{Ca_{M'} S_{Ca}^{N,X} + (\Sigma_{M'} - Ca_{M'}) S_{Na}^{N,X}}{(0.48 - Ca_{M'}) S_{Ca}^{N,X} + [0.52 - (\Sigma_{M'} - Ca_{M'})] S_{Na}^{N,X}}. \quad (3)$$

Two independent linear equations involving $\Sigma_{M'}$ and $Ca_{M'}$ are produced by substitution into Equation 3 of the respective values for peak ratios and "scattering powers," first for X- and then for N-radiation. The following values simultaneously satisfy those two equations:

¹ For the purposes of calculation involving no. 299B plagioclase, the 3% K in the M-cation site has been considered as Na so that $\Sigma Na = 0.52$ and $\Sigma Ca = 0.48$. This approximation is reasonable for neutron diffraction as $b_{Na} = 0.351$ and $b_K = 0.37$. For X-ray diffraction, the difference in scattering power between (1) 0.52 atoms of Na and (2) 0.49 Na + 0.03 K ranges from 0.22 to 0.11 e for $0.0777 < \sin \theta/\lambda < 0.806 \text{\AA}^{-1}$. Consequently, the error in the X-ray scattering model introduced by this approximation is negligible.

$$Ca_{M'} = 0.15(4) \quad Ca_{M''} = 0.33(4)$$

$$Na_{M'} = 0.29(7) \quad Na_{M''} = 0.23(7)$$

$$\Sigma_{M'} = \overline{0.44(3)} \quad \Sigma_{M''} = \overline{0.56(3)} \quad (4)$$

This model for occupancy is the most general solution for the M site in no. 299B plagioclase and has been used in both X and N refinements.

In order to establish the reliability of the difference Fourier analysis for the estimation of M-site occupancies, it was first necessary to show that both X-ray and neutron data sets modeled the An_{48} atomic positions precisely. A number of statistical tests have been used to analyze the structural models to confirm the absence of systematic bias between refined data sets. The results of these tests are given in Appendix 1.

Refinement procedure

Complementary information available from the X and the N refinement was used to advantage by performing structure refinements in the following sequence: (1) initial N refinement, (2) initial X refinement, (3) M-site model—isotropic thermal parameters, (4) M-site model—anisotropic thermal parameters, (5) final X refinement, (6) extinction in N refinement, and (7) occupancy refinements. These stages will now be described in some detail.

1. Initial N refinement. Atomic parameters from the structure of An_{28} (Phillips et al., 1971) were used as starting parameters for the program LINUS. A scale factor (applied to F_c), positional

Table 4. T-site bond lengths

T site	(1)	(2)	(3)
T ₁ O	1.679(1)	1.680(1)	0.51(1)
T ₁ M	1.657(1)	1.655(1)	0.32(1)
T ₂ O	1.653(1)	1.653(1)	0.32(1)
T ₂ M	1.654(1)	1.655(1)	0.32(1)

Note: Lengths (in Å) from (1) X-ray and (2) neutron data with (3) Al occupancies inferred using the method of Kroll and Ribbe (1983, p. 67) for plagioclase no. 299B with composition An₄₈.

and anisotropic thermal parameters of all atoms, and an isotropic Zachariasen extinction correction were refined. The M site was treated here as a single anisotropic Na-Ca atom. Al and Si were distributed randomly among the four T sites. Toward the end of this refinement stage, average bond lengths were calculated for each T site, and the Al-Si occupancies were reset according to the method of Kroll and Ribbe (1983, p. 67).

2. Initial X refinement. Final atomic parameters (including the single Na-Ca atom and T-site occupancies) from stage 1 were used as starting parameters for the X refinement. Positional, thermal, scale, and extinction parameters were then refined to minimize the function R_{2w} in program LINUS.

3. M-site model—*isotropic thermal parameters*. In both the X and N calculations, the extremely anisotropic character of the refined single M atom, as seen in the thermal parameters, indicated complexity in the structure of this site. In order to visualize the atomic distribution in the Na-Ca position, difference Fourier sections were prepared from both X and N data sets by excluding all contributions to F_c from the M site. The b-c section at $a = 0.26$ best illustrates the shape of the residual, which is quite similar for both X and N data. The difference Fourier section for X-ray data prepared at this refinement stage is reproduced in Figure 1a. The complex scattering distribution shown in this section cannot be adequately represented by a single M-atom model.

At this refinement stage, occupancies of a split-atom M site were calculated according to the procedure described above. Peak heights were taken from difference Fourier sections at $a = 0.26$ for both the N and the X data. Difference Fourier maps were generated using parameter values (including the scale factor) that resulted from stage 1 refinement for N data and stage 2 refinement for X data. However, the single anisotropic M atom was omitted from the model used for structure-factor calculation in both cases.

Site occupancies calculated from Equation 3 were assigned to the split-atom sites, and then positional and isotropic thermal parameters were refined with scale and isotropic extinction parameters. Near-equality of the refined isotropic temperature factors (i.e., $B_M^N \approx B_M^X$ and $B_M^X \approx B_M^N$) was used to check that calculated M-site occupancies (Eq. 4) were consistent with the initial assumptions about this site.

4. M-site model—*anisotropic thermal parameters*. Difference Fourier sections ($a = 0.26$) calculated after a further refinement cycle of positional and thermal parameters for all atoms include residuals around the Na-Ca positions as shown in Figure 1b. M' and M'' sites were consequently refined with anisotropic thermal parameters for both X and N data.

5. Final X refinement. Atomic parameters and esd's in Table 3 are from the final cycle of refinement, which included all parameters except for site occupancies. M-site occupancies were maintained at the values given in Equation 4. Direct refinements of T-site occupancies were not attempted owing to the similarity between Al and Si X-ray scattering factors. Final T-O bond lengths

Table 5. X-ray refinement statistics

	R_2^*	R_{2w}^*	GOF*	Refinement stage
(1)	0.095	0.113	8.655	2
(2)	0.083	0.095	7.152	3
(3)	0.038	0.056	4.335	5

Note: Statistics from (1) single anisotropic M atom, (2) two isotropic M atoms with Na-Ca distribution from Equation 4, and (3) two anisotropic M atoms with Na-Ca distributed according to Equation 4.

* See Table 2 for definitions.

and corresponding occupancies calculated by the method of Kroll and Ribbe (1983) are listed in Table 4.

X-ray refinement statistics are assembled in Table 5, and the final difference Fourier section is shown in Figure 1c.

6. Extinction in N refinement. The program RFINE4 (Finger and Prince, 1975) incorporating the extinction formalisms of Thornley and Nelmes (1974) was used at this stage. As the N crystal shape was somewhat irregular (viz., noncentric), the absorption weighted mean path length $T_{hkl} \neq T_{\bar{h}\bar{k}\bar{l}}$ and so the extinction corrected values $F_c(hkl) \neq F_c(\bar{h}\bar{k}\bar{l})$. It was therefore necessary to use a larger data set of 3185 reflections, in which hkl reflections were treated independently of $\bar{h}\bar{k}\bar{l}$ reflections. Initially, scale, isotropic extinction and all atomic positional and thermal parameters (two M sites) were refined to minimize the function R_w with weights w set at $1/\sigma^2(F_o)$ (see Table 6, line 4). Values of R_2 and R_{2w} were calculated for comparison with earlier refinement stages.

Then, simple type I and type II models for anisotropic extinction were refined by minimizing R_w using program RFINE4. Refinement statistics shown in Table 6 (lines 5 and 6) suggest that a type I model gives better agreement to the observed data.

Using the R-factor ratio test of Hamilton (1965), the type I anisotropic extinction model may be considered to be more appropriate than a model incorporating only isotropic extinction at least at the 99.9% confidence level.

The adequacy of anisotropic extinction was tested in two ways: (1) Strongly extinction-affected reflections were considered to be those with an extinction factor $y < 0.8$ (where y is the multiplier applied to F_c^2 prior to comparison with the observed values F_o^2 in an RFINE4 refinement). A total of 943 reflections in the N data set fell into this category. Type I anisotropic extinction, scale, and all atomic positional and thermal parameters were refined using this subset of strongly extinction-affected reflections (this

Table 6. Neutron-refinement statistics

	R^*	R_w^*	R_2^*	R_{2w}^*	GOF*	Refinement stage
1	—	—	0.094	0.110	3.103	1
2	—	—	0.091	0.107	2.956	3 LINUS**
3	—	—	0.073	0.090	2.548	4
4	0.056	0.052	0.084	0.102	3.08	6
5	0.051	0.043	0.074	0.086	2.59	6 RFINE**
6	0.048	0.038	0.065	0.076	2.29	6

Note: Statistics from (1) single anisotropic M atom, (2) two isotropic M atoms with Na-Ca distribution from Equation 4, (3) two anisotropic M atoms with Na-Ca distribution from Equation 4, (4) as for (3) but with isotropic extinction refined, (5) as for (3) but with type II anisotropic extinction, (6) as for (3) but with type I anisotropic extinction.

* See Table 2 for definitions.

** Program used in the corresponding refinement stage.

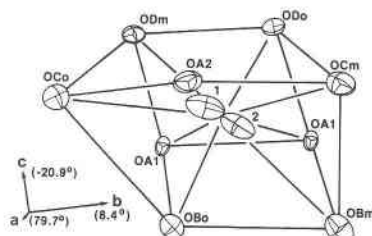


Fig. 2. Perspective view of the M-site environment from the final X-ray structure of no. 299B plagioclase (ORTEP plot, 98% probability ellipsoids). Orientation of the unit-cell axes is indicated at the lower left. Angle of inclination to the projection plane is shown for each axis with a positive angle denoting that the positive end of the corresponding axis lies above the projection plane. The unit-cell origin lies on the OA₁-OA₁ join. Labels 1 and 2 denote, respectively, atoms M' and M''.

refinement will be referred to as the partial refinement in the following text). Atomic parameters for the partial refinement differ by less than $3 \times$ esd from parameters refined using all reflections. Most parameter shifts were less than $2 \times$ esd (where the esd's are calculated from the partial refinement). The extinction ellipsoid (expressed in terms of Z_{ij} values) was also monitored. Its shape (axial ratios 1.34:1:0.45) and orientation did not change significantly, although the equivalent isotropic value of r^* increased from 3.5×10^{-4} in the full refinement to 4.1×10^{-4} in the partial refinement. The stability of extinction and atomic thermal parameters under these conditions is an indication of model adequacy (Coppens, 1978).

(2) Intensities of several of the strongly extinction-affected reflections were collected over a π -radian range of azimuthal angle. Sinusoidal-like fluctuations in measured intensity are consistent with anisotropic extinction. The effects of absorption of neutrons by the crystal ($\mu = 0.27 \text{ cm}^{-1}$) were calculated to be far too weak to produce the observed variations of intensity (e.g., $I_{\max}/I_{\min} = 1.5$ for the 060 reflection). Intensities were calculated for the appropriate diffractometer settings using the refined values of isotropic and anisotropic extinction parameters. In general, anisotropic type I extinction accounts for these observed intensity variations better than do isotropic or anisotropic type II extinction corrections. However, agreement between observed and calculated intensities is probably too poor to confidently discriminate between extinction models.

7. Occupancy refinements (N data). A direct refinement of the T- and M-site occupancies using the N data was attempted at this stage with type I anisotropic extinction. Each T site was constrained to be fully occupied and the Si content refined with no constraint on the total Si content of the T sites. After refinement, the Si content of the four T sites totaled 2.26(16) atoms of Si, equivalent to a plagioclase of composition $An_{74(\pm 16)}$. For the M sites, constraints were not placed on the occupancies as dictated by our general model of Na-Ca occupation. Therefore, only the scattering length of each M site was refined. After refinement, the sum of the scattering lengths for the two M sites was 0.406(10) cm^{-12} , equivalent to the M-cation chemistry of $An_{40(\pm 3)}$ plagioclase. Refined T- and M-site occupancies are clearly inconsistent with each other and with a bulk composition of An_{48} .

In addition, the value of R_w did not decrease with unconstrained refinement. The principal changes during cycles of unconstrained refinement were shifts in all M-site parameters, increases in the esd's of all M-site parameters and, to a lesser extent, of T-site thermal parameters. Final equivalent isotropic temper-

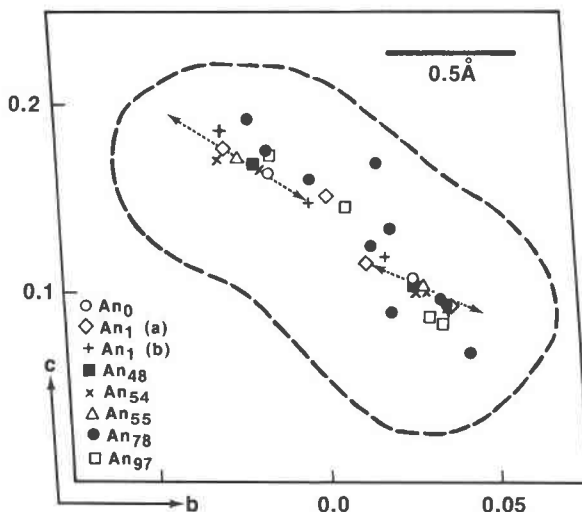


Fig. 3. M-site positions of various plagioclases converted to C₁ cell coordinates and projected parallel to the a axis onto a b-c section. Data have been taken from An₀—Winter et al. (1979), 2-site model; An₁(a)—Ribbe et al. (1969), 4-site model; An₁(b)—Prewitt et al. (1976); An₄₈—this study; An₅₄—Korekawa et al. (1979); An₅₅—Toman and Frueh (1976b); An₇₈—Kitamura and Morimoto (1977); and An₉₇—Czank et al. quoted by Smith (1974, vol. 1, p. 138). The two dashed arrows represent the projection of the displacement modulation wave vectors refined for both M positions of an An₅₅ structure by Toman and Frueh (1976b). The heavy dashed line encircling the plot is the first positive contour from the difference Fourier section of Fig. 1a.

ature factors for M' and M'' sites are also markedly different [$B(M') = 3.88 \text{ \AA}^2$ vs. $B(M'') = 1.81 \text{ \AA}^2$]. All of these results suggest that unconstrained refinement was unsuccessful.

Parameter sets produced from X- and N-data refinements, stages 5 and 6 respectively, have been used to generate observed and calculated structure-factor values (Tables 8 and 9) and tables of bond lengths and angles (Tables 10 and 11).²

M-site model

Final difference Fourier sections through an M site consisting of two unequal anisotropic atoms show significant residual densities for both X-ray (Fig. 1c) and neutron analyses of no. 299B plagioclase. The magnitudes of these residuals indicate that, although a two-position M site is definitely an improvement over a single site, it is still somewhat inadequate as a scattering model. A more accurate description of the site distribution may require a continuum of scattering matter, or at least a series of closely spaced cation sites. A notable feature of the initial Fourier sections (see Fig. 1a) is the slightly "dog-leg" shape of the residual density. This characteristic is also evident from the orientation of the refined thermal ellipsoids for the two partial M atoms shown in Figure 2.

² To obtain a copy of Tables 8–11, order Document AM-86-317 from the Business Office, Mineralogical Society of America, 1625 I Street, N.W., Suite 414, Washington, D.C. 20006, U.S.A. Please remit \$5.00 in advance for the microfiche.

The orientation of the overall M-site elongation itself gives no indication of the cause of positional disorder. Contrary to the conclusions of Kitamura and Morimoto (1975), we consider that, for plagioclases of a wide range of compositions, M-site positions (converted to an equivalent C1 cell) show indistinguishable trends (see Fig. 3). In addition, dispersion of the M-site positions for each plagioclase plotted in Figure 3 appears not to be correlated with bulk plagioclase composition. However, the overall trend of positions does conform well with the shape and orientation of the elongate scattering distribution in the no. 299B plagioclase M site; this has been demonstrated by reproducing in Figure 3 the trace of the first positive residual contour from the difference Fourier section of Figure 1a. We also note that this trend is in general agreement with the shape of the minimum-energy surface computed for high albite by Brown and Fenn (1979).

In the albite-like structure of no. 299B plagioclase, there are two alternative explanations for the M-site distribution:

1. Positional disorder characteristic of high albite. Although Prewitt et al. (1976) refined four partial sites, Winter et al. (1979) argued that the number of Na positions (based on the variety of possible configurations of neighboring Al-Si atoms) should not be limited to four. The complexity in the M site will be further increased with the introduction of significant amounts of Ca, as in the intermediate plagioclases.

2. Modulation of the M position. Modulation of the M position is described in current models of intermediate plagioclase by Toman and Frueh (1976b) and Kitamura and Morimoto (1977).

The presence of *e* reflections in diffraction patterns of no. 299B plagioclase support alternative 2. However, the coherence of any modulation in this crystal must be minimal, as implied by the weak and diffuse character of the superstructure reflections. On the other hand, the unmodulated nature of the TO₄ framework is shown by the isotropic nature of the thermal motion of T and O atoms. The axial ratios for the anisotropic displacement ellipsoids for no. 299B plagioclase (see Table 7) are not significantly different from the values for unmodulated low albite compiled by Smith (1974, Table 4-8). Such isotropic character suggests that proposal 1 may be appropriate. We conclude that both effects may contribute to the overall site disorder.

Asymmetry in the M site for no. 299B plagioclase is observed as a concentration of scattering in the M" site, as previously reported for plagioclase with compositions An₂₈ (Phillips et al., 1971) and An₆₂₋₆₆ (Wenk et al., 1980). No. 299B plagioclase has only weakly ordered T sites but unequal distribution of Ca over the two M sites (Eq. 4). Therefore, the partitioning of Ca into M' and M" sites for An₄₈ is believed not to be correlated with the degree of ordering of Al into the four T sites of this C1 average structure. Furthermore, this lack of correlation is consistent with the absence of systematic trends in the M-site asymmetries inferred from Fourier maps presented for

Table 7. Principal axes of anisotropic displacement ellipsoids for framework atoms derived from the final neutron parameters (see Table 3)

Atom label	RMS displacement (picometer)		
	X	Y	Z
T ₁ O	9.7	10.7	13.0
T ₁ M	9.7	10.1	13.8
T ₂ O	10.3	11.3	11.8
T ₂ M	10.3	10.9	11.6
OA1	10.6	16.4	18.3
OA2	12.0	12.4	14.6
OB0	12.9	14.9	17.4
OBM	12.1	17.5	20.3
OC0	13.4	15.3	16.1
OCM	12.1	13.6	18.8
ODO	11.7	15.5	16.7
ODM	11.8	15.8	19.8

four labradorites with different degrees of T-site ordering by Wenk et al. (1980, Fig. 5).

CONCLUSIONS

Extinction

In purely mathematical terms, the markedly anisotropic secondary extinction of the no. 299B crystal can be attributed to a rudimentary domain structure. It is surprising that this effect has not been reported in previous refinements of intermediate plagioclase. The anisotropic extinction corrections result in a significant improvement of the agreement between observed and calculated intensities, even though the F_o - F_c pairs for strongly extinction-affected reflections are poorly matched. A more sophisticated and general treatment of extinction, allowing for simultaneous primary and secondary type I and II corrections (such as that of Becker and Coppens, 1974), may result in better agreement for the strongly extinction-affected reflections.

T-O framework

There is good agreement between thermal and positional parameters derived from the X and from the N refinements (see Table 3). Axial magnitudes for ellipsoids of thermal vibration (Table 7) of the T and O sites are larger than those determined for some refinements of low-structural-state feldspars (Smith, 1974, vol. 1, p. 119) but agree closely with magnitudes derived from the refinement of high albite at 25°C by Winter et al. (1979).

Site-occupancy refinements

The value of R_w did not decrease with unconstrained refinement. In addition, values for T and M site occupancy derived from unconstrained refinement could not be reconciled with the known bulk composition of no. 299B plagioclase. For these and other reasons described in the stage 7 results section, the unconstrained refinement was considered unsuccessful, and the constrained occupancy model derived from Equations 3 and 4 was deemed the

most reliable available for the M-site chemistry. This M-site distribution is preferable to the variety of possible models based on ad hoc assumptions, either those implemented in previous studies or one such as $\Sigma_{M'} = \Sigma_{M''} = 0.5$.

T-site occupancies. Insignificant differences exist between T-O bond lengths calculated from final X and N refinements of atomic positions (Tables 4 and 10); hence a single set of individual T-site occupancies is assigned on the basis of bond length. Aluminum occupancies, determined directly by refinement of neutron-scattering lengths for the T sites differ by up to 3 esd's from the values calculated using bond lengths. The relative difference between neutron-scattering lengths for Al and Si is large enough to permit direct refinement in fully ordered low albite (Harlow and Brown, 1980). However, this difference would appear to be insufficient for accurate determination of the relatively weak T-site ordering in no. 299B plagioclase, and the bond-length-determined occupancies are to be preferred.

M-site occupancies (two-position M site). In this work the differences between the partial M sites are attributed primarily to a complex distribution of Na and Ca. In earlier work, Klein and Korekawa (1976) suggested a total partitioning of Na into the M' site (using our terminology) and Ca into the M'' site, whereas Wenk et al. (1980) presumed the ratio Na/Ca for M' was equal to that for M''. In each of these two cases, the refined thermal parameters for the two M sites are markedly different, i.e., $B(M') = 1.16 \text{ \AA}^2$ vs. $B(M'') = 2.02 \text{ \AA}^2$ for Klein and Korekawa (1976) whereas $B(M') = 3.66 \text{ \AA}^2$ vs. $B(M'') = 1.48 \text{ \AA}^2$ for the neutron refinement of Surtsey plagioclase by Wenk et al. (1980). Given the general M site approach we have developed in this paper, more reasonable thermal parameters $B(M') = 2.99 \text{ \AA}^2$ vs. $B(M'') = 2.59 \text{ \AA}^2$ can be obtained. Neither Klein and Korekawa's (1976) or Wenk et al.'s (1980) proposals appear valid for no. 299B plagioclase: the strong scattering in the An₄₈ M'' site (relative to the M' site) is due to *both* higher overall occupancy *and* a higher Ca content. The occupancy values calculated from our difference Fourier methods (Eq. 3) are more appropriate than those of our own unconstrained refinement (stage 7) or those derived from ad hoc assumptions about M-site chemistry. In addition, we believe that careful refinement of other intermediate plagioclases by the above method may well reveal similar M-site cation distributions.

Overall structure

In summary, the average C1 structure of this sample of An₄₈ includes an unmodulated framework of (Si_{2.52}Al_{1.48}O₈) with Al partially ordered into the T₁O site. Within this aluminosilicate framework lie positionally disordered Na-Ca sites whose occupancy and position are weakly correlated. The M-site disorder may be due in part to coherent modulations of the type that give rise to sharp *e*-reflections in low structural state plagioclase of intermediate composition. However, the total M-site disorder cannot be

completely explained by such modulations, and some component of positional disorder of the "high-albite type" is inferred for no. 299B plagioclase.

A comparison of difference Fourier sections generated during this study, and those of Phillips et al. (1971) and Wenk et al. (1980), indicates that there may be a correlation between the Ca content of the plagioclase and the ratio of the scattering in the M'' and M' sites. Thus, as the Ca content increases, so too does the scattering in the M'' site. This may be due to (1) Ca partitioning into the M'' site, (2) an increase in occupancy of this site, or (3) a combination of both effects. Further structural refinements using X-ray and neutron data, collected from plagioclase crystals at various temperatures, will be required to adequately define the major factors affecting the chemistry of the M sites.

ACKNOWLEDGMENTS

Since this study commenced in 1976, it has been technically and financially supported by the Australian Institute of Nuclear Science and Engineering (AINSE), its staff, in particular E. G. Palmer, F. H. Moore and R. L. Davis, and staff of the Australian Atomic Energy Commission, C. J. Howard and M. M. Elcombe. We are also indebted to the following: R. H. Vernon for providing the sample, I. Threadgold, B. M. Gatehouse and G. Fallon for making freely available their X-ray diffraction equipment and their expertise, and to C. Cuff, R. J. Hill, the late L. F. Power, P. H. Ribbe, and J. V. Smith for their encouragement.

Support is acknowledged by J.D.F.G. from an Australian Commonwealth Postgraduate Research Award, and by J.B.P. and I.D.R.M. from AINSE Postgraduate Awards. Tim Grove is thanked for his constructive review.

REFERENCES

- Abrahams, S.C., and Keve, E.T. (1971) Normal probability plot analysis of error in measured and derived quantities and standard deviations. *Acta Crystallographica*, A27, 157-165.
- Appleman, D.E., and Evans, H.T. (1973) Job 9214: Indexing and least-squares refinement of powder diffraction data. U.S. Geological Survey Computer Contributions, 20 (NTIS Document PB2-16188).
- Bacon, G.E. (1974) Neutron scattering amplitudes for elements and isotopes. In *International tables for X-ray crystallography*, volume IV, 270-271. Kynoch Press, Birmingham.
- Becker, P.J., and Coppens, P. (1974) Extinction within the limit of validity of the Darwin transfer equations. II. Refinement of extinction in spherical crystals of SrF₂ and LiF. *Acta Crystallographica*, A30, 148-153.
- Bloss, D.F. (1981) *The spindle stage; principles and practice*. Cambridge University Press.
- Brown, P.E., and Fenn, P.M. (1979) Structure energies of the alkali feldspars. *Physics and Chemistry of Minerals*, 4, 83-100.
- Coppens, Phillip. (1974) Some implications of combined X-ray and neutron diffraction studies. *Acta Crystallographica*, B30, 255-261.
- (1978) Combined X-ray and neutron diffraction: The study of charge density distributions in solids. In H. Dachs, Ed. *Neutron diffraction*, 71-111. Springer-Verlag, New York.
- Coppens, Phillip, and Hamilton, W.C. (1970) Anisotropic extinction corrections in the Zachariasen approximation. *Acta Crystallographica*, A26, 71-83.
- Cromer, D.T., and Waber, J.T. (1974) Scattering factors for X-rays. In *International tables for X-ray crystallography*, volume IV, 270-271. Kynoch Press, Birmingham.
- Deer, W.A., Howie, R.A., and Zussman, J. (1966) *An introduction to the rock-forming minerals*. Longman, London.

- Finger, L.W., and Prince, E. (1975) A system of Fortran IV computer programs for crystal structure computations. U.S. National Bureau of Standards Technical Note 854.
- Grove, T.L. (1977) A periodic antiphase structure model for the intermediate plagioclases (An₃₃ to An₇₅). *American Mineralogist*, 62, 932–941.
- Grove, T.L., Ferry, J.M., and Spear, F.S. (1983) Phase transitions and decomposition relations in calcic plagioclase. *American Mineralogist*, 68, 41–59.
- Hamilton, W.C. (1965) Significance tests of the crystallographic R-factor. *Acta Crystallographica*, 18, 502–510.
- Harlow, G.E., and Brown, G.E. (1980) Low albite: An X-ray and neutron diffraction study. *American Mineralogist*, 65, 986–995.
- Hashimoto, Hatsujiro, Nissen, H.-U., Ono, A., Kumao, A., Endoh, H., and Woensdregt, C.F. (1976) High-resolution electron microscopy of labradorite feldspar. In H.-R. Wenk, Ed. *Electron microscopy in mineralogy*, 332–344. Springer-Verlag, New York.
- Hawthorne, F.C., and Grundy, H.D. (1976) The crystal chemistry of the amphiboles. IV: X-ray and neutron refinements of the crystal structure of tremolite. *Canadian Mineralogist*, 14, 334–345.
- Hornstra, J., and Stubbe, B. (1972) PW1100 data processing program. Philips Research Laboratories, Eindhoven.
- Horst, W., Tagai, Tokuei, and Korekawa, Masaaki. (1981) Modulated structure of a plagioclase An₅₂: Theory and structure determination. *Zeitschrift für Kristallographie*, 157, 233–250.
- Kitamura, Masao, and Morimoto, Nubuo. (1975) The superstructure of intermediate plagioclase. *Japanese Academy Proceedings*, 51, 419–424.
- (1977) The superstructure of plagioclase feldspars. A modulated coherent structure of the e-plagioclase. *Physics and Chemistry of Minerals*, 1, 199–212.
- Klein, S., and Korekawa, Masaaki. (1976) Die Gemittelte Struktur des Labradorits. *Neues Jahrbuch für Mineralogie Monatshefte*, 2, 66–69.
- Korekawa, Masaaki, Horst, W., and Tagai, Tokuei. (1979) Structure determination of plagioclase (labradorite) II. The superstructure of a plagioclase An₅₄ (X-ray diffraction). In J.M. Cowley, J.B. Cohen, M.B. Salamon, and B.J. Wuensch, Eds. *Modulated structures—1979*. American Institute of Physics Conference Proceedings 53, section 6, 312–313.
- Kroll, Herbert. (1983) Lattice parameters and determinative methods for plagioclase and ternary feldspars. *Mineralogical Society of America Reviews in Mineralogy*, 2 (2nd edition), 101–120.
- Kroll, Herbert, and Ribbe, P.H. (1983) Lattice parameters, composition and Al/Si order in alkali feldspars. *Mineralogical Society of America Reviews in Mineralogy*, 2 (2nd edition), 57–99.
- Kumao, A., Hashimoto, Hatsujiro, Nissen, H.-U., and Endoh, H. (1981) Ca and Na positions in labradorite feldspar as derived from high-resolution electron microscopy and optical diffraction. *Acta Crystallographica*, A37, 229–238.
- Morimoto, Nubuo. (1979) The modulated structures of feldspars. In J.M. Cowley, J.B. Cohen, M.B. Salamon, and B.J. Wuensch, Eds. *Modulated structures—1979*. American Institute of Physics Conference Proceedings 53, section 6, 299–310.
- Phillips, M.W., Colville, A.A., and Ribbe, P.H. (1971) The crystal structures of two oligoclases: A comparison with low and high albite. *Zeitschrift für Kristallographie*, 133, 43–65.
- Prewitt, C.T., Sueno, Shigeho, and Papike, J.J. (1976) The crystal structure of high albite and monalbite at high temperatures. *American Mineralogist*, 61, 1213–1225.
- Ribbe, P.H. (1983) Chemistry, structure and nomenclature of feldspars. *Mineralogical Society of America Reviews in Mineralogy*, 2 (2nd edition), 1–20.
- Ribbe, P.H., Megaw, H.D., Taylor, W.H., Ferguson, R.B., and Traill, R.J. (1969) The albite structures. *Acta Crystallographica*, B25, 1503–1518.
- Smith, J.V. (1974) *Feldspar minerals. Volume 1—Crystal structure and physical properties and Volume 2—Chemical and textural properties*. Springer-Verlag, Berlin.
- Thornley, F.R., and Nelmes, R.J. (1974) Highly anisotropic extinction. *Acta Crystallographica*, A30, 748–757.
- Toman, Karel, and Frueh, A.J. (1976a) Modulated structure of an intermediate plagioclase—I. Model and computation. *Acta Crystallographica*, B32, 521–525.
- (1976b) Modulated structure of an intermediate plagioclase—II. Numerical results and discussion. *Acta Crystallographica*, B32, 526–538.
- Wenk, H.-R. (1978) Ordering of the intermediate plagioclase structure during heating. *American Mineralogist*, 63, 132–135.
- Wenk, H.-R., Joswig, Werner, Tagai, Tokuei, Korekawa, Masaaki, and Smith, B.K. (1980) The average structure of An_{62–66} labradorite. *American Mineralogist*, 65, 81–95.
- Winter, J.K., Ghose, Subrata, and Okamura, F.P. (1977) A high-temperature study of the thermal expansion and the anisotropy of the sodium atom in low albite. *American Mineralogist*, 62, 921–931.
- Winter, J.K., Okamura, F.P., and Ghose, Subrata. (1979) A high-temperature structural study of high albite, monalbite, and the analbite → monalbite phase transition. *American Mineralogist*, 64, 409–423.

MANUSCRIPT RECEIVED DECEMBER 17, 1984

MANUSCRIPT ACCEPTED JULY 8, 1986

APPENDIX 1.

COMPARISON OF X-RAY AND NEUTRON REFINED PARAMETERS

A number of statistical tests can be used to analyze structural models for evidence of systematic bias between refined data sets. Two useful tests of systematic bias are (1) half-normal probability tests and (2) χ^2 tests. Abrahams and Keve (1971) have shown that normal probability plot analysis can be applied to independent sets of crystallographic structure-factor measurements (F) and their derived atomic coordinates (p). Differences between pairs of positional or thermal parameters (Δp) can be examined in terms of their pooled standard deviations (σp) by plotting the ordered statistic $\delta p = \Delta p / \sigma p$ against the expected normal distribution. For correctly assigned standard deviations and a normal

error distribution between experiment and model, a half-normal probability plot will be linear with unit slope and zero intercept. Deviation from linearity suggests some systematic difference between the parameter sets. Gross errors in individual δp will be seen at that extremity furthest from the origin of each half-normal plot.

Figures A1 and A2 are half-normal probability plots for the positional and thermal parameters from independent neutron and X-ray refinements of plagioclase no. 299B. The distribution of points in Figure A1 shows that there is no obvious systematic bias between the X-ray and neutron positional parameters. The pooled standard deviations for positional parameters are underestimated by a factor of ~1.5. The thermal parameter plot (Fig. A2) shows a deviation from linearity only at the high- δp end. The slope of the half-normal plot in Figure A2 is approximately

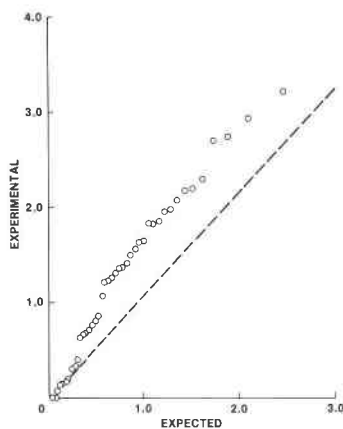


Fig. A1. Half-normal probability plot for refined positional parameters of plagioclase no. 299B. The dashed line represents an ideal normal distribution of δp_i . The linearity of the experimental points indicates that the δp_i is approximately normally distributed.

3.5 and indicates that the pooled standard deviations for thermal parameters are considerably underestimated. The curvature of the half-normal probability plot in Figure A2 suggests that there may be some bias between the thermal parameter sets. The existence of bias is confirmed by the χ^2 tests discussed below.

In addition to half-normal probability-plot analysis, χ^2 tests may be used to examine the differences between individual sets of parameters (Hamilton, 1965). The method involves an application of the well known χ^2 test to the sum of the weighted differences between two experiments. The function

$$R^2 = \sum_{i=1}^N R_i^2$$

may be tested as χ^2 , where $R_i = \Delta_i \sigma_i$, for $\Delta_i = p(1)_i - p(2)_i$, and $\sigma_i = [\sigma p(1)_i^2 + \sigma p(2)_i^2]^{1/2}$ for two data sets, each with N parameters, $p(1)_1, \dots, p(1)_N$ and $p(2)_1, \dots, p(2)_N$.

Table A1 lists the χ^2 values of positional and thermal parameters for the plagioclase no. 299B X-ray and neutron refinements. The calculated R^2 values for positional parameters lie within the range $\chi_{n,95}^2 < R^2 < \chi_{n,5}^2$. (R_n^2 , the χ^2 value for the x positional

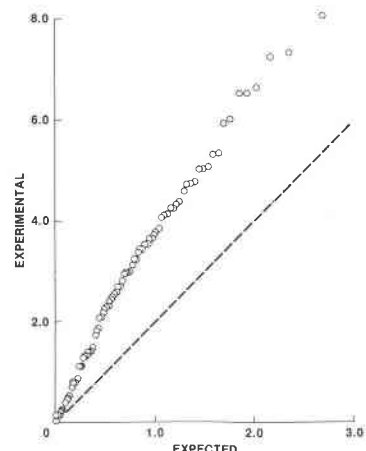


Fig. A2. Half-normal probability plot for plagioclase no. 299B refined thermal parameters. (Note that the slope of the reference line here equals 2). The deviation from linearity of experimental points suggests that some systematic bias exists between the X-ray and neutron thermal parameters.

parameter, actually lies outside the range of χ^2 by an amount almost equivalent to the interpolation error in calculating $\chi_{42,5}^2$.) Thus, the χ^2 tests for positional parameters are consistent with the analysis of half-normal probability plots for the two independent data sets.

For plagioclase no. 299B, the χ^2 test of thermal parameter subsets is a more revealing test than the half-normal probability test. The χ^2 test for thermal parameters shows that no value of $R_{\beta ij}^2$ lies within the range $\chi_{84,95}^2 < R_{\beta ij}^2 < \chi_{84,5}^2$. Thus, at the 5% level, all thermal parameter subsets (i.e., $\beta_{11}, \dots, \beta_{23}$) indicate some systematic difference between the two experiments. Systematic differences between experiments may arise if (1) the σ values are too small in one or both experiments, (2) there are real differences between the true values of the experiments, or (3) an incorrect model has been refined in one or both experiments. For the plagioclase no. 299B X-ray and neutron experiments, systematic bias in thermal parameters probably arises from (1) low σ values and (2) the inadequacy of X-ray scattering factors to approximate the atomic charge cloud (Coppens, 1974; Hawthorne and Grundy, 1976).

It is apparent from these statistical tests of the refined X-ray and neutron parameters that there is no significant difference between their atomic positions. The excellent correspondence between the X-ray and neutron positional parameters for plagioclase no. 299B can be further confirmed by inspection of Table 3. All of the differences between corresponding values in the two parameter sets are less than one esd, and this is for data sets in which, incidentally, the esd's are underestimated.

As might have been expected, anisotropic thermal parameters from X-ray and neutron refinements do not show the desirable normal distribution of differences—some systematic bias does exist between the refined thermal parameter sets. However, this bias in anisotropic thermal parameters will not affect the calculation of M-site occupancies.

Table A1. Results of χ^2 tests comparing X-ray- and neutron-refined parameters for the no. 299B plagioclase structures

Positional parameters	Thermal parameters		
$R_x^2 = 27.27$	$R_{\beta_{11}}^2 = 198.70$	$R_{\beta_{12}}^2 = 52.63$	
$R_y^2 = 30.91$	$R_{\beta_{22}}^2 = 513.07$	$R_{\beta_{13}}^2 = 127.68$	
$R_z^2 = 36.99$	$R_{\beta_{33}}^2 = 133.29$	$R_{\beta_{23}}^2 = 15.07$	
$\chi_{42,95}^2 \approx 57.78$		$\chi_{84,95}^2 \approx 106.64$	
$\chi_{42,5}^2 \approx 27.86$		$\chi_{84,5}^2 \approx 64.65$	